Available online at www.sciencedirect.com

ScienceDirect

Scripta Materialia 94 (2015) 36–39

Scripta MATERIALIA

www.elsevier.com/locate/scriptamat

Cooling rates and peak temperatures during friction stir welding of a high-carbon steel

V. Manvatkar,[a] A. De,[a] L.-E. Svensson[b] and T. DebRoy[a,*]

[a]*The Pennsylvania State University, University Park, PA, USA*
[b]*Production Technology Center, University West, Trollhattan, Sweden*

Received 22 July 2014; revised 29 August 2014; accepted 1 September 2014
Available online 26 September 2014

Friction stir welding can potentially avoid the need for post weld heat treatment for the welding of high-carbon steels. Although control of both peak temperature and cooling rate has been suggested to achieve this goal, the current literature does not provide any help with selecting appropriate welding variables. In order to address this problem, here we present a set of easy-to-use maps of both the cooling rates and the peak temperatures for various welding conditions during friction stir welding of a high-carbon steel.

Keywords: High-carbon steel; Friction stir welding; Cooling rates; Peak temperatures

The welding of high-carbon steels by fusion welding often results in the degradation of ductility and requires subsequent heat treatment to mitigate the harmful effects of martensite formation. A possible recourse is to weld these steels by friction stir welding (FSW). FSW has been used for the welding of various types of steels including the high-carbon varieties [1–12]. Friction stir welded joints of an interstitial-free steel are characterized by finer microstructure and higher strength compared to joints produced by gas tungsten arc welding [8]. The yield strength of joints produced by friction stir welding of a 0.11 wt.% C carbon steel, ST37, with an austenitic stainless steel, SS304, were higher than both the base alloys. The higher strength was attributed to a fine microstructure comprised of pearlite and ferrite [9]. However, the ultimate tensile strength of the joint was higher than that of ST37 steel but lower than that of SS304 steel [9]. Chung et al. [4,10] and Cui et al. [11] examined the feasibility of welding high-carbon steels by FSW. Cui et al. [11] observed martensite in the microstructure of the weld zone during FSW of a 0.72 wt.% C carbon steel and suggested ways to avoid its formation. They proposed selection of appropriate welding variables to maintain the peak temperature below the A_1 temperature or a cooling rate lower than the critical cooling rate for the formation of martensite [11]. Chung et al. [4] avoided martensite formation during FSW of a 0.85 wt.% C carbon steel by maintaining the stir zone temperature below the A_1 temperature of the alloy. However, the current literature does not provide any guidance on selecting welding variables to prevent loss of ductility. Reliable maps of cooling rates and peak temperatures for various welding variables are needed, but are not currently available.

Experimental measurements of a large number of peak temperatures and cooling rates during FSW of high-strength steels are time consuming and expensive. A practical recourse is to use a set of experimental data to adequately test and validate a comprehensive phenomenological model of heat transfer and material flow and subsequently use the model to calculate the necessary cooling rates and peak temperatures. Aeronautical, mechanical, civil and other engineers now routinely use numerical heat transfer and material flow models in critical designs.

Comprehensive numerical heat transfer and material flow models of friction stir welding have been developed and tested by several groups of researchers [13–20]. These models involve solving the equations of conservation of energy, mass and momentum for steady-state conditions considering incompressible viscous flow. Spatially variable local values of heat generation rates and viscosity of the plasticized material are calculated using appropriate sub-models [14–16]. These models have correctly predicted the experimentally measured peak temperature and thermal cycles [13–19], traverse force [20–22] and torque [18–22] in FSW of aluminum alloys [18,20–23], steels [15,16] and a titanium alloy [17,20]. Since the models and their applications are described in detail in the literature, they are not repeated here. Instead a model is validated for the FSW of a high-carbon steel and subsequently used to understand the roles of important welding parameters on the peak temperatures,

* Corresponding author; e-mail: rtd1@psu.edu

http://dx.doi.org/10.1016/j.scriptamat.2014.09.012
1359-6462/

cooling rates and microstructures of the stir zone of a high-carbon steel.

The numerical model is first validated by comparing the computed thermal cycles with the corresponding experimentally measured thermal cycles during FSW of a high-carbon steel at two different tool rotational speeds [11]. Subsequently, the numerically computed peak temperatures and cooling rates are presented as functions of welding speed and the rate of heat input in the form of easy-to-use contour maps. The estimated values of the rate of heat input as function of tool shoulder diameter and rotational speed are also plotted to determine their influence on the peak temperature and cooling rate. The computed peak temperatures and cooling rates are also used to understand the stir zone microstructure of a high-carbon steel for different welding conditions. This is the first paper to provide a practical means to estimate peak temperatures and cooling rates for various welding parameters.

Tables 1 and 2 indicate the temperature-dependent material properties of the 0.72 wt.% C carbon steel [24] and the welding conditions [11] used in the calculations. Figure 1 shows a comparison of the computed and the corresponding measured [11] thermal cycles during FSW of this steel for two different tool rotational speeds at a constant welding speed. The thermal cycles were monitored at the bottom surface of the workpiece below the tip of the tool pin. The computed peak temperatures in Figure 1 are 907 and 1230 K for tool rotational speeds of 200 and 800 rpm, respectively, which agree well with the corresponding experimentally determined values. The good agreement between the numerically computed and the corresponding experimentally measured thermal cycles shows that the model can be used to calculate the peak temperatures and cooling rates during FSW of the 0.72 wt.% C carbon steel.

The peak temperature and cooling rates are examined as function of the rate of heat generation, Q, which can be analytically calculated using the expression suggested by Schmidt et al. [25]:

$$Q = \frac{2}{3}\pi[\delta\tau + (1-\delta)\mu P] \times \omega[(R_S^3 - R_P^3)(1+\tan\alpha) + R_P^3 + 3R_P^2 H_P], \quad (1)$$

where δ is related to the slip between the shoulder and the workpiece material, τ is the shear yield strength of workpiece material, μ is the friction coefficient, P is the axial pressure, ω is the angular speed, R_S is the shoulder diameter, α is the shoulder cone angle, and Rp and H_P are the pin radius and length, respectively. The values of δ and μ were taken as 0.31 and 0.49, respectively [15,16]. These values are based on previous research [15,16]. However, the effects of variations of δ and μ on the computed peak temperature and cooling rate were examined for a 1.6 mm thick 0.72 wt.% C carbon steel. It was found that when δ was varied between 0.27–0.34 and μ was varied between 0.44–0.53, the computed peak temperatures were in the range of 1146–1156 K and the cooling rates varied between 72–77 K s^{-1} at a tool rotational speed of 500 rpm and welding speed of 6.667 mm s^{-1}. These results indicate that the effects of variation of μ and δ on the computed peak temperatures and cooling rates are small. Figure 2 shows a map of the calculated rate of heat generation as function of tool rotational speed and shoulder diameter. For example, the rate of heat generation changes from 0.95 to 8.0 kW for tool rotational speeds of 100–800 rpm, respectively, for the experimental conditions of Cui et al. [11]. The heat generation rate increases with increase in both the tool shoulder diameter and the tool rotational speed as expected.

Figure 3a,b shows the computed peak temperature at the top and bottom regions of the stir zone as function of welding speed and the rate of heat generation in a 1.6 mm thick steel plate containing 0.72 wt.% C. The results show that the peak temperature increases with an increase in the heat generation rate. This plot can also be used to understand the effect of welding speed. At faster welding speeds, the peak temperature decreases because of lower heat input per unit length. For a given rate of heat input, the difference in peak temperature between the top and bottom of the stir zone increases with increase in the welding speed. Figure 3 also shows that the peak temperature in the stir zone remains below A_1 temperature (996 K) of the 0.72 wt.% C carbon steel at lower rate of heat generation, i.e. at tool rotational speed of 100 rpm or lower. This martensite-free region is marked by cross-hatching in both Figures 3a and b. For all other welding conditions, the peak temperature exceeds the A_1 temperature at least at the top surface as shown in Figure 3a. The results show that some austenite will form in the stir zone which may convert to martensite if the weld experiences a high cooling rate. It is, therefore, necessary to estimate the cooling rate in the stirred zone.

Figure 4 shows the contours of the numerically computed cooling rates between 1073 and 773 K for various

Table 1. Material properties of the workpiece and the tool used for numerical calculations [24].

Property	Workpiece [11]	WC-based tool [11]
ρ (kg m^{-3})	7860	19,400
k (W m^{-1} K^{-1})	$71.86 - 0.0729T + 3.09 \times 10^{-5} T^2$	$92.3 + 124.67\exp(-T/580.93)$ 92.09 for T ⩾ 2000 K
C (J kg^{-1} K^{-1})	$989 - \frac{490}{1+(T/902)^{7.55}}$	$128.50 + 3.41 \times 10^{-6} T^2 + 3.28 \times 10^{-2} T$
τ (MPa)	$3.4 + \frac{286.4}{1+\exp(\frac{T-935}{60})}$	57.7

Table 2. Workpiece dimension and process parameters used for numerical calculations [11].

Workpiece dimensions, mm	Tool dimensions, mm			Welding conditions	
(length × width × thickness)	Shoulder diameter	Pin diameter	Pin length	Rotational speed, rpm	Welding speed, mm s^{-1}
300 × 30 × 1.6	12	4	1.5	100–900	0.42–7.08

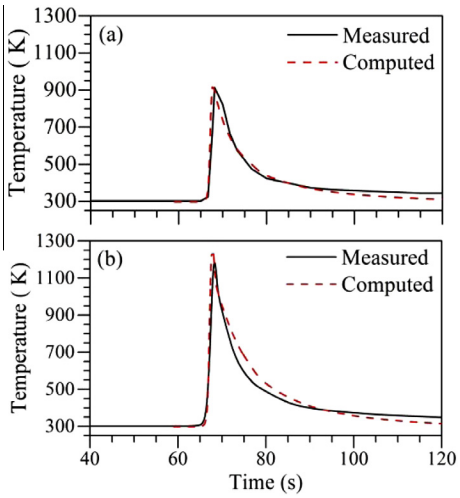

Figure 1. A comparison of the computed and the experimentally measured [11] thermal cycles at the bottom surface of the workpiece along the weld center line during FSW of a 1.6 mm thick, 0.72 wt.% C carbon steel. The welding speed was 6.667 mm s^{-1} and the tool rotational speeds were 200 rpm for (a), and 800 rpm for (b).

welding speeds and heat generation rates. The computed cooling rates are similar to those reported in the published literature for FSW of steels [7,12,26]. The cooling rate increases significantly with the increase in the welding speed and decreases gradually with the increase in the rate of heat input. At higher welding speeds, the heat input per unit length of the weld decreases and, as a result, the weld metal cools faster. In contrast, a slower rate of cooling is observed for higher heat generation rates at a constant welding speed. This behavior is similar to fusion welding where an increase in heat input results in slower cooling because of the finite rate of transport of the extra heat.

The critical cooling rate for martensite formation is 16 K s^{-1} for a steel containing 0.72 wt.% C, 0.7 wt.% Mn and 0.2 wt.% Si [27]. In Figure 4, this threshold value is shown by the 16 K s^{-1} cooling rate contour and the cross-hatched region indicates the martensite-free domain. Figure 4 shows that the cooling rates are higher than this critical cooling rate for welding speeds higher than 1 mm s^{-1}. This welding speed is fairly low and martensite formation is anticipated for faster welding speeds. This result is consistent with the experimental findings of Cui et al. [11]. They reported an increase in the volume fraction of martensite from 16% to 97% in the stir zone when the

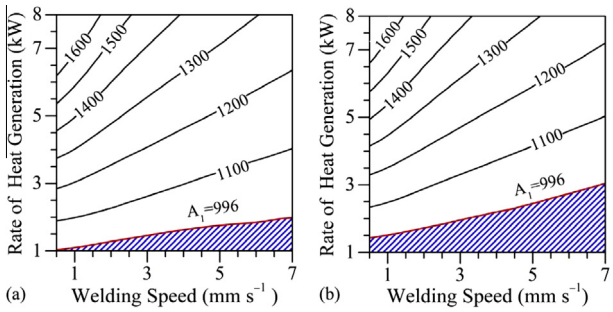

Figure 3. Contours of computed peak temperature (K) for FSW of a high-carbon steel [11] as function of welding speed and rate of heat generation at (a) top and (b) bottom of the stir zone.

welding speed increased from 0.42 to 6.67 mm s^{-1} [11]. At a rotational speed of 200 rpm and welding speed of 6.67 mm s^{-1}, the volume fraction of martensite was nearly 40% but martensite was observed only in the upper part of the stir zone. The results in Figure 3 show that the bottom region of the stir zone remained below the A_1 temperature. The measured thermal cycle in Figure 2a [11] also confirms the calculated results and the microstructural observation.

Cui et al. [11] observed martensite formation only in the upper part of the stir zone for a tool rotational speed of 200 rpm, welding speed of 6.67 mm s^{-1} and shoulder diameter of 12 mm [11]. For this experimental condition, the rate of heat generation is ~1.8 kW as shown in Figure 2. Figure 3 shows that at this heat generation rate, only the top region of the stir zone exceeds the A_1 temperature. All other regions remain below the A_1 temperature. Figure 4 shows that the cooling rate would be above 70 K s^{-1} for these experimental conditions. Since the temperature of the top region in the stir zone exceeds the A_1 temperature and the cooling rate is higher than the critical cooling rate, the observed martensite formation is consistent with the computed results. The measured thermal cycle in Figure 1a [11] also confirms the calculated results and the microstructural observation.

Cui et al. [11] also reported coarsening of martensite structure in the stir zone when welding was done at the highest rotational speed of 800 rpm in comparison to the weld made at 400 rpm, both at the maximum welding speed of 6.67 mm s^{-1}. Figure 2 shows that the rates of heat generation correspond to approximately 7 and 4 kW for tool rotational speeds of 800 and 400 rpm, respectively, for a given shoulder diameter of 12 mm. The resulting peak

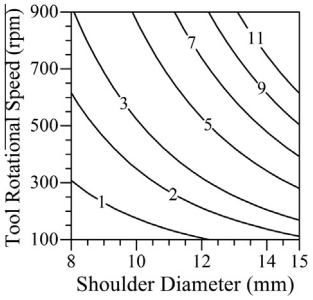

Figure 2. Contours of the estimated rate of heat generation (kW) as function of tool rotational speed and shoulder diameter during FSW of a high-carbon steel.

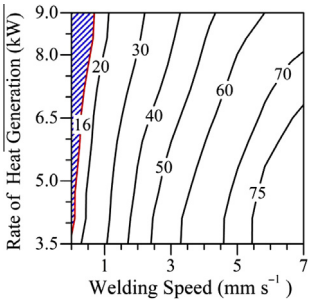

Figure 4. Contours of the computed cooling rate (K s^{-1}) between 1073 and 773 K for FSW of a high-carbon steel [11] as function of welding speed and rate of heat generation in the stir zone.

temperatures at the top of the stir zone are approximately 1300 and 1100 K, respectively, for 800 and 400 rpm as indicated in Figure 3. The coarsening of stir zone microstructure at 800 rpm can therefore be attributed to the higher peak temperature that has been also anticipated by Cui et al. [11]. These authors also reported that the martensitic structure was not observed at very low rotational speed of 100 rpm. The estimated rate of heat generation at 100 rpm with a shoulder diameter of 12 mm is ~0.95 kW and Figure 3 clearly shows that the peak temperature in the stir zone would remain below the A_1 temperature (996 K) for this welding condition. Defect-free welds were obtained at both 100 and 200 rpm with a welding speed of 25 mm min^{-1}.

Figures 3 and 4 can be used further to explain the observed weld joint microstructure in the FSW of steels of similar composition. For example, Chung et al. [4] observed both martensite and pearlite, with the martensite fraction decreasing from the top to the bottom in the stir zone during FSW of 0.85 wt.% C carbon steel at a tool rotational speed and welding speed of 400 rpm and 3.33 mm s^{-1}, respectively. In contrast, the stir zone microstructure was entirely ferritic at a much lower rotational speed of 100 rpm. Figure 3 indicates that the peak temperature would remain well below the A_1 (999 K) temperature for very low rates of heat generation at a tool rotational speed of 100 rpm. Thus, a ferritic microstructure in the stir zone is expected. In contrast, the peak temperature in the stir zone is expected to remain well above the A_1 temperature and reduce from the top to the bottom by nearly 50 K at a welding speed of 3.33 mm s^{-1} and rotational speed of 400 rpm ($Q \approx 3.77$ kW). In addition, Figure 4 indicates a reasonably high cooling rate corresponding to this welding condition. As a result, martensitic transformation is less likely at the bottom of the stir zone than at the top.

In summary, the computed results from a well-tested three-dimensional heat transfer and material flow model show that the model can predict peak temperatures and cooling rates for the FSW of high-carbon steels for various welding conditions. The computed results are used to construct contour maps of peak temperatures and cooling rates in the temperature range 1073–773 K for the FSW of a 0.72 wt.% C carbon steel. These maps are able to reveal the effects of welding variables. The computed results show that the martensite formation can be prevented only at fairly low rate of heat generation. The cross-hatched regions of Figures 3 and 4 show the welding parameter ranges that avoid martensite formation. Furthermore, it is easier for martensite to form in the upper region of the stir zone than at the lower region.

We wish to thank Dr. Snehanshu Pal of The Pennsylvania State University for his interest in this research.

[1] W.M. Thomas, P.L. Threadgill, E.D. Nicholas, Sci. Technol. Weld. Joining 6 (1999) 365.
[2] T.J. Lienert, W.L. Stellwag Jr., B.B. Grimmett, R.W. Warke, Weld. J. 82 (2003), 1-s.
[3] H. Fujii, L. Cui, N. Tsuji, M. Maeda, K. Nakata, K. Nogi, Mater. Sci. Eng. A 429 (2006) 50.
[4] Y.D. Chung, H. Fujii, R. Ueji, N. Tsuji, Scr. Mater. 63 (2010) 223.
[5] L.Y. Wei, T.W. Nelson, Weld. J. 90 (2011), 95-s.
[6] R. Nandan, T. DebRoy, H.K.D.H. Bhadeshia, Prog. Mater. Sci. 53 (2008) 980.
[7] H.K.D.H. Bhadeshia, T. DebRoy, Sci. Technol. Weld. Join. 14 (2009) 193.
[8] A.K. Lakshminarayanan, V. Balasubramanian, J. Mater. Eng. Perform. 20 (2011) 82.
[9] M. Jafarzadegan, A. Abdollah-Zadeh, A.H. Feng, T. Saeid, J. Shen, H. Assadi, J. Mater. Sci. Technol. 29 (2013) 367.
[10] Y.D. Chung, H. Fujii, R. Ueji, K. Nogi, Sci. Technol. Weld. Join. 14 (2009) 233.
[11] L. Cui, H. Fujii, N. Tsuji, K. Nogi, Scr. Mater. 56 (2007) 637.
[12] M. Ghosh, K. Kumar, R.S. Mishra, Metall. Mater. Trans. A. 43 (2012) 1966.
[13] P.A. Colegrove, H.R. Shercliff, R. Zettler, Sci. Technol. Weld. Joining 12 (2007) 284.
[14] R. Nandan, G.G. Roy, T. DebRoy, Metall. Mater. Trans. A 37A (2006) 1247.
[15] R. Nandan, G.G. Roy, T.J. Lienert, T. DebRoy, Sci. Technol. Weld. Joining 11 (2006) 526.
[16] R. Nandan, G.G. Roy, T.J. Lienert, T. DebRoy, Acta Mater. 55 (2007) 883.
[17] R. Nandan, T.J. Lienert, T. DebRoy, Int. J. Mater. Res. 99 (2008) 434.
[18] M. Mehta, A. Arora, A. De, T. DebRoy, Metall. Mater. Trans. A 42A (2011) 2716.
[19] V.D. Manvatkar, A. Arora, A. De, T. DebRoy, Sci. Technol. Weld. Joining 17 (2012) 460.
[20] A. Arora, M. Mehta, A. De, T. DebRoy, Int. J. Adv. Manuf. Technol. 61 (2012) 911.
[21] A. Arora, R. Nandan, A.P. Reynolds, T. DebRoy, Scr. Mater. 60 (2009) 13.
[22] A. Arora, A. De, T. DebRoy, Scr. Mater. 64 (2011) 9.
[23] A. Arora, T. DebRoy, H.K.D.H. Bhadeshia, Acta Mater. 59 (2011) 2020.
[24] W.F. Gale, T.C. Totemeier, Smithells Metals Reference Book, eighth ed., Elsevier, ASM, 2004.
[25] H. Schmidt, J. Hattel, J. Wert, Modell. Simul. Mater. Sci. Eng. 12 (2004) 143.
[26] A. De, H.K.D.H. Bhadeshia, T. DebRoy, Mater. Sci. Technol. 30 (2014) 1050.
[27] M. Atkins, Atlas of Continuous Cooling Transformation Diagrams for Engineering Steels, British Steel Corporation, 1977.